Measurement report: Contrasting elevation-dependent changes in light absorption of black and brown carbon: lessons from *in-situ* measurements from highly polluted Sichuan Basin to pristine Tibetan Plateau

Suping Zhao[1,2,3,4], Shaofeng Qi[1,6], Ye Yu[1,2,3], Shichang Kang[4], Longxiang Dong[1,2,3], Jinbei Chen[1,2,3], Daiying Yin[5,6]

[1] Key Laboratory of Land Surface Process and Climate Change in Cold and Arid Regions, Northwest Institute of Eco-Environment and Resources, Chinese Academy of Sciences, Lanzhou 730000, China
[2] Pingliang Land Surface Process & Severe Weather Research Station, Pingliang, 744015, China
[3] Gansu Land Surface Process & Severe Weather Observation and Research Station, Pingliang, 744015, China
[4] State Key Laboratory of Cryospheric Science, Northwest Institute of Eco-Environment and Resources, Chinese Academy of Sciences, Lanzhou 730000, China
[5] Key Laboratory of Desert and Desertification, Northwest Institute of Eco-Environment and Resources, Chinese Academy of Sciences, Lanzhou 730000, China
[6] University of Chinese Academy of Sciences, Beijing 100049, China

Correspondence to: Suping Zhao (zhaosp@lzb.ac.cn); Daiying Yin (yindaiying@lzb.ac.cn)

Abstract. The scientific knowledge on light absorption of aerosols is extremely limited at the eastern slope of the Tibetan Plateau (ESTP). We conducted the first aerosol field experiment at six sites (Chengdu, Sanbacun, Wenchuan, Lixian, Maerkang, Hongyuan) along the ESTP extending elevation from 500 m to 3500 m. The light absorption of brown carbon (BrC) accounting for that of total carbon increases from 20% to 50% with altitude, and the mass absorption efficiency (MAE) of BrC over the TP is 2–3 times higher than that inside the SiChuan Basin (SCB), especially in winter. Contrary to BrC aerosols, winter EC (elemental carbon) mass absorption efficiency declines with altitude. The contrasting variation of EC and BrC MAE with altitude is mainly attributed to source difference between the TP and SCB. The more urban sources (motor vehicles, industries, etc.) inside the SCB fail to be transported to the TP due to winter stable air inside the basin, which also is favorable for aerosol aging to enhance absorption efficiency. The radiative forcing of BrC relative to EC varies from 0.10 to 0.42 as altitude increases with the higher OC/EC ratio over the TP than SCB, and thus the enhanced radiative forcing of BrC relative to EC from polluted SCB to pristine TP is because the concentration of OC decreases more slowly with altitude than does EC. This study will deepen the understanding of EC

or BrC light absorption difference between the highly polluted basins and clean TP and provide a basic data set for optimization of regional climate modeling.

1 Introduction

Some *in-situ* observations, available satellite data and model simulations indicated that greater surface warming trend over time occurs at higher altitudes for the mountainous regions all over the world (Gao et al., 2018; Guo et al., 2019; Mountain Research Initiative EDW Working Group, 2015; Palazzi et al., 2017; Pepin et al., 2019; Rangwala and Miller, 2012; You et al., 2020). Rangwala and Miller (2012) reviewed elevation-dependent warming (EDW) and its possible causes over four high mountain regions, i.e., the Swiss Alps, the Colorado Rocky Mountains, the Tibetan Plateau and the Tropical Andes. Their examinations found that the available observations indicate that some mountain regions show much greater warming rates at seasonal scales. The mechanisms that can produce enhanced warming rates at higher altitudes may be related to differential sensitivities of surface warming to changes in the climate drivers at different elevations, such as snow-ice cover, clouds, atmospheric water vapor, aerosols, land use, and vegetation (Rangwala and Miller, 2012; You et al., 2020).

Tibetan Plateau (TP, hereafter), known as “third pole”, is an ideal place to examine EDW and its mechanism (Guo et al., 2021). The warming rates (rising temperature per 10 years) over TP are found to be the most notable in winter and autumn (Liu and Chen, 2000), especially for the central and eastern Plateau (Duan and Wu, 2006), which may be partly associated with human activities, such as more anthropogenic emissions at the sub-regions (Lu et al., 2010). The effect of carbonaceous aerosols on regional and even global climate is more uncertain due to short life than the long-lived ones, such as carbon dioxide and methane (Chung et al., 2012; Ramanathan and Carmichael, 2008). The absorbing aerosols (black carbon and dust) from local emissions or long-range transport heat the atmosphere in two ways (Tian et al., 2018). They absorb radiation and decrease the surface albedo when deposited on snow and ice (Kang et al., 2019; Lau et al., 2010; Xu et al., 2009). Ramanathan and Carmichael (2008) suggested that black carbon (BC) in the Himalayas arising from anthropogenic activities at Indo-Gangetic Plain could account for half of the local warming during the past several decades. In addition to the well-known BC, the recent work by Wu et al. (2018) suggested that the light absorption efficiency (LAE) of brown carbon (BrC, certain type of organic aerosols) in winter is 2-3 times higher

than that in summer for the central Tibetan Plateau. However, the scientific knowledge on optical properties of carbonaceous aerosols (EC, BrC) is extremely limited over the eastern TP, and *in-situ* aerosol measurements at varying altitudes from the heavily polluted basins to the relatively clean TP were important for better understanding their light absorption.

The previous *in-situ* measurements mainly focused on the southern and northern slopes (Cong et al., 2015; Huang et al., 2007; Kang et al., 2020), while fewer observations were conducted at the eastern slope of the TP (ESTP). SiChuan Basin (SCB), a highly polluted region in China due to more rapid economic development, is located on the east side of TP (Zhao et al., 2018). The BrC LAE was strong inside the basin (Peng et al., 2020a), especially for the rural areas due to more biomass and coal burning impacts (Zhao et al., 2021). Our previous works indicated that aerosols from SCB are transported upslope along ESTP and reach eastern part of TP by gradient *in-situ* observations at ESTP (Yin et al., 2020). The recent study by S. Y. Zhao et al. (2020) suggested the strong light-absorbing BrC from biomass and coal burning inside the basin can be transported to main part of TP by the enhanced "heat pump" in response to rapid warming over the TP. The aerosols over the TP from local emissions and long-range transport from the surrounding highly polluted areas affected its weather, climate and water cycle (C. F. Zhao et al., 2020). The clouds and radiation are particularly sensitive to aerosols over pristine regions (Garrett and Zhao, 2006; Zhang et al., 2021). However, it is fuzzy that the light absorption and radiative forcing of carbonaceous aerosols change from the highly polluted SCB to the cleaner TP.

In this work, we investigated the changes in light absorption of carbonaceous aerosols (EC, BrC) and calculated relative radiative forcing of BrC to EC aerosols from SCB to TP in the four seasons. The sources and origins also were determined by some statistical methods and HYSPLIT back trajectory model. Our goals are to understand EC or BrC light absorption difference between the highly polluted basins and clean TP and to reveal the corresponding mechanisms and to provide a basic data set for optimization of regional climate modeling.

2 Data and methods

2.1 Observation sites and aerosol sampling

Compared with the coarser fraction of PM, strong light-absorbing carbonaceous particles are mainly located in submicron range. Therefore, PM_1 (particulate matter with aerodynamic diameter smaller than 1 μm) samples were collected at six sites (Chengdu, Sanbacun, Wenchuan, Lixian, Maerkang and Hongyuan) from western SCB to east part of TP with varying elevation from 500 m to 3500 m (Figure 1, Table 1). Each sampling site is selected to represent background level at local scale as completely as possible without local emission impacts. The 1024 PM_1 samples in total were collected from December 21, 2018 to December 18, 2019 on a day / night pattern by aerosol sampler (LY-2034, Laoying Instrument Co., Ltd., China) at the flow rate of 100 L min^{-1}. The samples were stored frozen in prebaked glass jars until further analysis (Kawamura et al., 2010). The meteorological variables (temperature, relative humidity, wind speed and direction) were downloaded by China Meteorological Data Service Center (http://data.cma.cn/). PM_1 samples were collected near the meteorological observation sites, and thus the meteorological variables can represent the situation at the study region. The MODIS active fire data (https://earthdata.nasa.gov/active-fire-data) also were used in this study.

2.2 Chemical analysis

A quarter of each filter was used to analyze water-soluble inorganic ions (Na^+, NH_4^+, K^+, Ca^{2+}, Mg^{2+}, F^-, Cl^-, SO_4^{2-}, and NO_3^-), and the ions were extracted and filtered by ultrapure water and a 0.45 μm pore syringe filter. The concentrations of the cations and anions were measured by ion chromatograph (DX-600 & ICS-2500, Dionex, USA). The carbonaceous aerosols, i.e., organic carbon (OC) and elemental carbon (EC), were determined by a seven-wavelength carbon analyzer (Model-2015, DRI, USA). The carbon analyzer measured OC and EC concentrations using the thermal/optical reflectance (TOR) method (Chow et al., 2007). Briefly, the OC / EC was determined by progressively heating the sub-filter. The OC fractions were determined by heating at 120 °C (OC1), 250 °C (OC2), 450 °C (OC3) and 550 °C (OC4) in a pure He atmosphere; subsequently, EC fractions were measured at 550 °C (EC1), 700 °C (EC2) and 800 °C (EC3) in an oxidizing atmosphere of 2% O_2 and 98% He. The involved carbon is oxidized to CO_2 and then reduced to CH_4 for detection by a flame ionization detector. The pyrolyzed organic carbon (OPC) was monitored when the reflected laser signal returned to its initial

value after introducing O_2 to the analysis atmosphere. The OC was defined as the sum of OC1, OC2, OC3, OC4 and OPC while EC was defined as EC1 + EC2 + EC3 − OPC. EC and BrC were derived from light absorption coefficient (b_{abs}) depending on transmittance attenuation. For the seven-wavelength carbon analyzer, the filter transmittance (FR_λ, fraction of light transmitted through the filter) uncertainties range from 5% to 18%, with the best precision shown at 450 nm and 808 nm (Chen et al., 2015). The uncertainty is attributed to the quality of the laser and the sensitivity of the photodiode detector for different wavelengths.

The coefficient of variation (CV) in conjunction with correlation coefficients (r) can be used to characterize intra-location variability of chemical species (Zhao et al., 2021). CV is calculated by the below equation:

$$CV_{jk} = \sqrt{\frac{1}{p}\sum_{1}^{p}\left(\frac{x_{ij} - x_{ik}}{x_{ij} + x_{ik}}\right)^2}, \quad (1)$$

where x_{ij} and x_{ik} are the average concentration for a chemical component *i* at sites *j* and *k*, and *p* is the number of samples. The CV values of zero and approaching one mean no difference and absolute heterogeneity between the two sites for the specific chemical component, respectively. The CV lower than 0.2 is usually considered to represent relatively similarity of spatial pattern (Wang et al., 2018).

2.3 Calculation of light absorption parameters

The BrC light absorption increases sharply as decreased wavelength, and thus it can be separated from EC (Peng et al., 2020a). The light absorption induced by carbonaceous aerosols (sum of EC and BrC) on a quartz filter was estimated by an algorithm of transmittance attenuation (*ATN*):

$$ATN_\lambda = \ln\left(\frac{FT_{\lambda,a}}{FT_{\lambda,b}}\right), \quad (2)$$

where, $FT_{\lambda,a}$ and $FT_{\lambda,b}$ in the right hand represent filter transmittance after and before thermal analysis for the specific wavelength (λ). Referring to the work by Chen et al. (2015), the relation of ATN with absorption optical depth (τ_a) can be given as follows,

$$\tau_{a,\lambda} = a_\lambda \times ATN_\lambda^{\,2} + c_\lambda \times ATN_\lambda \quad (3).$$

This study used the two coefficients (a_λ and c_λ) reported by Chen et al. (2015). The light absorption

coefficients (b_{abs}) can be calculated with the equation:

$$b_{abs,\lambda} = \tau_{a,\lambda} \times \left(\frac{A}{V}\right), \quad (4)$$

where, *A* and *V* are filter area and sampling volume, respectively. The total b_{abs} can be separated into EC and BrC by a simplified two-component model (Chen et al., 2015):

$$b_{abs,\lambda} = b_{abs,\lambda,EC} + b_{abs,\lambda,BrC} = K_1 \times \lambda^{-AAE_{EC}} + K_2 \times \lambda^{-AAE_{BrC}}, \quad (5)$$

where, K_1 and K_2 are fitting coefficients. AAE_{EC} and AAE_{BrC} represent EC and BrC absorption Ångström exponent (AAE), respectively. They do not change as the wavelength. AAE_{EC} was assumed as 1 (Bond, 2001), and the other three parameters in Eq. (5) were obtained for AAE_{BrC} values between 2 and 8 with the increment of 0.1 by least-square linear regression, and the AAE_{BrC} that led to the overall best fit in terms of R^2 was selected as the effective BrC AAE. The mass absorption efficiency (MAE) was obtained by the ratio of light absorption coefficients ($b_{abs,\lambda,EC}$ or $b_{abs,\lambda,BrC}$) to the corresponding EC or OC mass concentrations (Olson et al., 2015). The estimated MAE_{BrC} was much lower than the true value by replacing BrC with OC due to BrC accounting for only a small fraction of OC. The main shortcoming of the separation of total aerosol absorption into EC and BrC (Eq. 5) is lack of considering the mineral dust impacts. According to the recent study of Zhang et al. (2021), mineral dust may be an important species of the atmospheric aerosols over the Tibetan Plateau. However, the study region is located at the eastern slope of TP during our campaign, which is more easily affected by anthropogenic sources from heavy polluted Sichuan Basin than natural sources such as mineral dust (Yin et al., 2020) as compared to the north areas close to Taklimakan and Gobi Deserts. One main aim of this study is to reveal the gradient distributions of aerosol optical properties from the pollution Sichuan Basin to eastern TP, and thus the impact of the shortcoming may be negligible when studying the spatial heterogeneity of aerosol optical properties at relatively small spatial scale. In addition, AAE of EC is assumed as 1, and the aging of EC did not take when separating the total aerosol absorption into EC and BrC (Eq. 5) in our study.

The absorbed light by carbonaceous component can be estimated as follows (Huang et al., 2018):

$$\frac{I_0 - I}{I_0}(\lambda, EC) = 1 - e^{-\left(MAE_{\lambda 0,EC} \times \left[\frac{\lambda_0}{\lambda}\right]^{AAE_{EC}} \times C_{EC} \times PBLH\right)} \quad (6)$$

$$\frac{I_0 - I}{I_0}(\lambda, BrC) = 1 - e^{-\left(MAE_{\lambda 0,BrC} \times \left[\frac{\lambda_0}{\lambda}\right]^{AAE_{BrC}} \times C_{OC} \times PBLH\right)}, \quad (7)$$

where, 405 nm is determined as reference wavelength λ_0, and C_{EC} and C_{OC} represent EC and OC concentrations, respectively. The planetary boundary layer height (PBLH) was obtained from the HYSPLIT model, and we assumed no vertical gradients within the PBL. The assumption might overestimate the radiative forcing of aerosols, while it has small effect on the radiative forcing of BrC relative to EC (*f*), which can be estimated by the below equation (Zhao et al., 2019):

$$f = \frac{\int I_0(\lambda)\left[\frac{I_0 - I}{I_0}(\lambda, BrC)\right] d\lambda}{\int I_0(\lambda)\left[\frac{I_0 - I}{I_0}(\lambda, EC)\right] d\lambda}, \quad (8)$$

where $I_0(\lambda)$ is wavelength-dependent solar emission flux, which is clear sky Air Mass 1 Global Horizontal solar irradiance (Levinson et al., 2010). The light absorption by BrC at 405 nm and 445 nm is much stronger than that at the longer wavelength inside the SCB (Zhao et al., 2021). The 405 nm is the lower limit of detection by the instrument of DRI-2015. Therefore, the fraction (*f*) is obtained by numerical integration of the above formula at the wavelength range of 405-980 nm and 405-445 nm for each sample, respectively. The nighttime samples were excluded when calculating the radiative forcing of BrC relative to EC.

The exponential function was selected to fit the relationships between BrC MAE and altitude (*AT*). The equation is given as follows:

$$MAE_{\lambda,BrC} = a_\lambda \cdot e^{b \times AT}, \quad (9)$$

where, a_λ and *b* are the fitted coefficients. The EC MAE can be parameterized with altitude by replacing the subscript of *BrC* with *EC* in Eq. (9).

2.4 HYSPLIT backward trajectory model

HYbrid Single-Particle Lagrangian Integrated Trajectory (HYSPLIT) model developed by the National Oceanic and Atmospheric Administration's (NOAA) is a complete system for computing simple air parcel trajectories (Draxler et al., 2009). HYSPLIT continues to be one of the most extensively used atmospheric transport and dispersion models. A common application is a back trajectory analysis to determine the origin of air masses and establish source-receptor relationships. In this study, HYSPLIT

model was used to determine potential source regions of air pollutants in the four seasons at the six sites. The 96-h backward trajectories arriving at 500 m above ground level (AGL) and initializing at each hour of day were calculated with $0.25^{\circ}\times0.25^{\circ}$ Global Data Assimilation System (GDAS) data from National Centers for Environmental Prediction (NCEP). The gridded back trajectory frequencies were calculated with Openair package of Rplot.

2.5 PMF receptor model

EPA PMF receptor model (version: 5.0) is a mathematical approach for quantifying the contribution of sources to samples based on the composition or fingerprints of the sources. A speciated data set can be viewed as a data matrix X of *i* by *j* dimensions, in which *i* number of samples and *j* chemical species were measured, with uncertainties *u*. The goal of PMF model is to solve the chemical mass balance between measured species concentrations and source profiles, as shown in the below Eq. (10), with number of factors *p*, the species profile *f* of each source, and the amount of mass *g* contributed by each factor to each sample:

$$x_{ij} = \sum_{k=1}^{p} g_{ik} f_{kj} + e_{ij}, \quad (10)$$

where e_{ij} is the residual for each sample/species. In this study, the uncertainties of the chemical species concentrations were estimated by the Eq. (11):

$$Unc = \sqrt{\left(0.1\times concentration\right)^2 + \left(0.5\times MDL\right)^2}, \quad (11)$$

where MDL is species-specific method detection limit. The water-soluble ions and carbonaceous aerosols in the four seasons at the six sites were used as input variables to run PMF model. The MDL of the species can refer to Cui et al. (2019).

3 Results and discussion

3.1 Light absorption of EC and BrC

Table2 summarizes seasonally mean OC and EC concentrations, light absorption coefficient and efficiency (b_{abs}, MAE) of EC and BrC at 405 nm and the meteorological variables at the six sites during the campaign. The average winter EC concentration ranges from 2.2 μg m^{-3} at Maerkang to 7.9 μg m^{-3} at Sanbacun, which is about 2–6 times higher than those in the other seasons in response to more

primary emissions in winter with similar wind speeds (Table2). The much higher OC/EC ratios at the plateau sites than that at the basin sites suggests that more secondary OC is formed by chemical reactions over the TP, which can be supported by the works of Wu et al. (2018). The higher OC/EC ratios with the altitude can also result from stronger EC emissions at lower altitudes. Combined with the previous studies, the winter OC concentration is found to vary from 15.0 to 20.1 μg m^{-3}, while EC is between 4.3 and 4.7 μg m^{-3} at urban areas inside the SCB, which is significantly lower than that at Indo-Gangetic Plain (Table S1). However, OC and EC concentrations at eastern TP are much more abundant than that at western and southern TP sites due to more dense population and industry (Table S1). Briefly, carbonaceous aerosol pollution is much more severe inside the basin than that over the TP, indicating that the large amount of air pollutants is trapped inside the deep basin due to calm and stable air.

Figure 2 compares spectral total and separated EC and BrC b_{abs} in spring and winter at the six sites along the ESTP. The measured (green hollow points) and calculated b_{abs} (yellow dash lines) for total carbon (TC, sum of EC and BrC) is comparable, and the difference is within 5%. For Sanbacun, a rural site inside the basin, the b_{abs} is much higher than the other sites, especially for the shorter wavelength due to more BrC emissions from coal and biomass burning for cooking and heating at rural areas inside the SCB (Zhao et al., 2021). The light absorption of EC aerosols decreases with altitude primarily because of declined EC concentration (see Table2). The phenomenon may be partly due to stable air inside the deep basin (Feng et al., 2020), but that would also apply to BrC in so far as EC and BrC share sources, and vertical mixing is primarily due to fair weather convection rather than deep convective storms (Zhang et al., 2017). However, the light absorption by BrC does not monotonically change as altitude due to more complicated sources and origins of BrC. The 405 nm b_{abs} of BrC accounting for that of TC increases from 20% at Chengdu to ~ 50% at Hongyuan, while the proportion significantly reduces with increased wavelength (Figure S1), suggesting that light absorption of BrC aerosols is much stronger at high altitudes than that at lowlands.

Compared with b_{abs}, MAE can better reflect light absorption efficiency of aerosols. The average winter MAE_{EC} is 6.0±1.0 m^2 g^{-1} among all sites, which is within the range of 3.9–11.9 m^2 g^{-1} over the TP and the surrounding basins (Tables2 and S1). Except our result in the rural site, the mean winter MAE_{BrC} of

0.7–0.8 m^2 g^{-1} inside the SCB is about half of that at Indo-Gangetic Plain (IGP) probably due to the differences in BrC emissions, PM size distribution and chemical composition between SCB and IGP (Choudhary et al., 2018). Figures 3 and S2 show box plots of spectral MAE_{BrC} and MAE_{EC} in the four seasons from the basin to plateau sites extending elevation from 0.5 to 3.5 km. Different from EC, MAE_{BrC} at 405 nm over the TP is 2–3 times higher than that inside the SCB with strong elevation-dependent light-absorbing, and the only clear dependence is in winter. Wu et al. (2018) found that winter MAE_{BrC} is 4.5 m^2 g^{-1} for a pristine environment over the TP (Nam Co, 4730 m asl), which is significantly higher than that at Hongyuan (3500 asl) for our study. The average winter OC/EC ratio of 14.1 at Nam Co is largely higher than that at our sampling sites. Therefore, the clearly increased winter MAE_{BrC} with altitude may be related to BrC composition seasonally, while winter MAE_{EC} decreases with altitude possibly due to the difference in source composition and aging aerosols inside the deep basin (Liu et al., 2020). The mechanism will be discussed in the following sections.

Figure 4 shows MAE_{BrC} and MAE_{EC} variations as altitude in spring and winter during the campaign. The relationships between average MAE and altitude of the measurement sites were fitted by exponential function, and coefficients of determination (R^2) were given in the figure. R^2 reflects the strength of the relationships between two parameters. The contrasting MAE variation as altitude between BrC and EC in winter (R^2 of 0.89 for MAE_{BrC} and 0.86 for MAE_{EC}) is more significant than those in spring (R^2 of 0.45 for MAE_{BrC} and 0.06 for MAE_{EC}). The better relationships in winter may be because more urban and aged aerosols are trapped inside the deep basin in response to strong winter temperature inversion (Feng et al., 2020). The relation of MAE_{BrC} or MAE_{EC} at 405 nm with altitude can be parameterized with exponential function (Eq. 9). The spring and winter MAE_{BrC} can be parameterized with altitude (*AT*) as follows:

$$MAE_{405,BrC,spr} = 1.33 \cdot e^{0.18 \cdot AT} \quad (12)$$

$$MAE_{405,BrC,win} = 0.82 \cdot e^{0.33 \cdot AT} \quad (13).$$

Similarly, the winter MAE_{EC} can be parameterized by altitude (*AT*) as follows:

$$MAE_{405,EC,win} = 11.35 \cdot e^{-0.18 \cdot AT} \quad (14).$$

3.2 Sources impacting on light absorption of EC and BrC

OC/EC ratio can be used to roughly identify sources of carbonaceous aerosols, and the ratio of aerosols from fossil combustion is generally lower than that of biomass burning (Bond et al., 2004). Figure S3 shows the relationship between OC and EC concentrations inside the SCB and that over the TP during the campaign, and OC/EC ratio was obtained by fitting the relationships with univariate linear regression. The significantly simultaneous change between OC and EC (R^2 = 0.80 for SCB, and R^2 = 0.75 for TP) indicated that the sources may be similar. OC/EC ratio of 2.14 for western SCB and 2.06 for eastern TP are significantly lower than that at Nam Co (13.8–14.1, Wu et al., 2018) representing a pristine environment over central TP (Cong et al., 2009), while the ratios are much higher than that at Lhasa, the largest city over TP (1.46, Li et al., 2016). The OC/EC ratio for our study is slightly lower than that at urban areas in eastern China and Helsinki in Finland (Han et al., 2014; Viidanoja et al., 2002), indicating that carbonaceous aerosols at western SCB and eastern TP may be significantly affected by primary sources.

Besides primary sources, secondary formation largely contributes to OC aerosols, and thus secondary organic carbon (SOC) was calculated with EC-tracer method (Turpin and Lim, 2001). To better understand light absorption of primary and secondary OC, Figures S4 and 5 show sample-to-sample and average MAE_{BrC} variations as SOC and POC concentrations for each site in spring and winter during the campaign, respectively. The light absorption efficiency of BrC significantly declines as the increased OC composition with the better relationships for POC at each site (Figure S4). The average winter MAE_{BrC} decreased by about 70% as POC increases from 3.0 μg m^{-3} at Hongyuan to higher than 20 μg m^{-3} at Chengdu (Figure 5). SOC accounting for OC significantly increases from western SCB to eastern TP, and it is higher than 50% at Maerkang and Hongyuan due to relatively fewer primary sources over the TP. The large winter MAE_{BrC} increment as SOC/POC ratio indicates that the more SOC and the fewer POC are favorable for BrC light absorption enhancement (Figure 5). Therefore, the strong elevation-dependent MAE_{BrC} in winter (Figure 4) may be induced by SOC/POC ratio variations from the western SCB to eastern TP.

The EC light absorption efficiency largely reduces as EC concentrations increase at each site (Figure S5). However, the average winter MAE_{EC} inside the highly polluted SCB is much higher than that over

the clean TP, while for similar EC concentrations among the plateau sites, MAE_{EC} at Wenchuan is about 2 times higher than that at Hongyuan with strong dependence on elevation. Therefore, winter aerosol aging inside the deep basin and large source differences may induce light absorption reduction from the western SCB to eastern TP. The increase of MAE_{EC} as the ratios of water soluble ions (K^+, Cl^-, SO_4^{2-}, and NO_3^-) to EC concentrations on different levels suggests that EC light absorption is certainly impacted by many anthropogenic sources at the six sites (Figure S6). A specific inorganic component can be considered as the indicator of the specific emission sources. K^+ and Cl^- ions are usually used for characterizing biomass burning (BB) and coal combustion (CC), respectively (Tao et al., 2016). NO_3^- and SO_4^{2-} can reflect motor vehicle and industry source impacts, respectively. Therefore, to further find key sources impacting MAE_{EC}, we check the spring and winter mean MAE_{EC} variations as the concentrations of K^+, Cl^-, NO_3^- and SO_4^{2-} ions at the six sites (Figure 6). Compared with the spring value, the winter MAE_{EC} is the lower due to high EC concentrations and more sensitive to the chemical species from anthropogenic emissions. Furthermore, NO_3^- difference among the sites (Figure 6a) is much larger than K^+, Cl^- and SO_4^{2-} due to many fossil fuel combustion at Chengyu City Clusters inside the basin. The spatial heterogeneity in $(NO_3^- + SO_4^{2-}) / (K^+ + Cl^- + NO_3^- + SO_4^{2-})$ ratio in winter is more significant than that in spring, and winter MAE_{EC} obviously increases as the ratio from TP to the basin sites. Therefore, the emissions from fossil fuel combustion may be a key source influencing winter MAE_{EC}.

The above paragraphs separately analyzed light absorption efficiency of BrC and EC and their variations as chemical species, while the change in radiative forcing of BrC relative to EC (*f*) from Chengdu to Hongyuan is showed in Figure 7a to reveal the mechanism. The parameter (*f*) reflects light absorption strength of BrC at the shorter wavelengths as compared to that of EC aerosols at the whole wavelengths. The much higher *f* values indicated that radiative forcing of BrC aerosols is much stronger for the similar EC radiate forcing, and thus this parameter can be used to better understand the radiative forcing of secondary aerosols relative to primary aerosols at a specific location. The altitude (*AT*) increased by 3 km, while the median *f* increases from about 0.10 inside the basin to 0.42 over eastern TP. The relationship between *f* and altitude can be parameterized as the below equation:

$$f = 0.077 \cdot e^{0.480 \cdot AT} \quad (15).$$

Some studies found that the direct radiative forcing of BrC / (BrC+EC) increases with altitude simply due to the fact that the concentration of BrC decreases more slowly with altitude than does EC (Liu et al., 2014, 2015; Zeng et al., 2020; Zhang et al., 2017). Therefore, we also checked the median OC/EC ratio variations from the basin to plateau sites during the campaign (Figure 7b). The OC/EC ratio changes within the range of 2–4, and the 75th percentiles of the ratio increases more significantly than the median values from the basin to plateau sites. Therefore, the increased *f* from western SCB to eastern TP may be closely related to more secondary formation and fewer primary emissions over the TP than SCB (also see Figure 5c).

As previously mentioned, MAE of carbonaceous aerosols largely depends on emission sources. PMF receptor model is widely used to apportion the sources influencing air pollutants at a specific site based on the fingerprints of the sources, for example K^+ and Cl^- are usually used as tracer for biomass burning (BB) and coal combustion (CC), respectively (Tao et al., 2016). PMF analysis was conducted in this study for each season. The motor vehicles, biomass and coal burning, dust, sea salt and secondary formation are found to be the main sources at the six sites. Figure 8 shows mass concentrations of species for each source at each site apportioned by PMF model in winter during the campaign. The PMF results for the other seasons are illustrated in Figures S7–S9. The winter NO_3^- concentrations for secondary nitrate decrease from 3.44 μg m^{-3} at Sanbacun to 0.07 μg m^{-3} at Maerkang, which is more heterogeneous than that in summer and fall. As a main source inside the SCB, the winter secondary nitrate is in response to the intensive mixing between the motor vehicle emissions and other primary pollutants trapped inside the basin by strong capping inversion (Feng et al., 2020). Additionally, high humidity inside the SCB facilities the secondary nitrate formation, and the average nitrogen oxidation ratio in Sichuan (average RH = 80%) is 3.1 times of that in winter Beijing (average RH = 27%) (Wang et al., 2021). EC aerosols from the intensive human activities inside the SCB are easily aged by coating the secondary formed nitrate in winter, which further causes the enhancement of basin EC light absorption. The latest studies of Zhang et al. (2022) found that light absorption and radiative forcing of black carbon coated by inorganic salts are much stronger than that inside organic materials. The chemical species (K^+, Cl^-) from biomass burning and coal combustion decline from the basin to plateau sites, but the declining ranges in warm seasons (summer and fall) are more significant than those in the cold seasons (spring and winter) due to usage of more fuel for

heating over the TP. Therefore, the primary BrC from biomass burning and coal combustion for winter heating over the TP may partly contribute to the strong TP BrC light absorption.

3.3 Impacts of regional and long-range transport on the light absorption of aerosols

The fresh aerosol particles are gradually aged by mixing with other pollutants during the long-range transport, and then enhance their light absorption and radiative forcing. The similarities of major chemical species between two sites should represent regional air pollution, while the differences should reflect local source impacts. The comparisons between basin (Chengdu, Sanbacun) and plateau sites (Wenchuan, Lixian, Maerkang, Hongyuan) about the average mass concentrations of water-soluble ions and carbonaceous species in the four seasons are showed in Figures 9 and S10–S12. The numerical ranges between the two axes of each subplot are set to be equal to more clearly see spatial heterogeneity of the chemical species at the region. The combination of CV with correlation coefficients can be used to better understand intra-location variability (Wilson et al., 2005). The CV is between 0 and 1 (see Eq. 1), and the smaller value represents the more uniform particle concentrations. The moderate differences, relatively high CV values (0.22–0.75), are observed for the chemical species from anthropogenic sources (NH_4^+, K^+, SO_4^{2-}, NO_3^-, F^-, Cl^-, OC, and EC) in the four seasons. The differences indicated that there are limited similarities between basin and plateau sites, and the discrepancies were in major anthropogenic sources. The spatial heterogeneity for K^+ and NO_3^- is more obvious than the other species in the four seasons, which is mainly related to more biomass burning and vehicle emissions inside the SCB (Zhao et al., 2021). The weak inter-region transport between western SCB and eastern TP suggested that the light absorption of carbonaceous aerosols over the TP is rarely influenced by pollutants from the SCB. Furthermore, the CV values for K^+, NO_3^-, and EC in winter are the lowest among the seasons due to increased biomass burning and coal combustion for winter heating over Tibetan Plateau. Unlike CV, high correlation coefficient for the specific chemical component does not necessarily indicate uniformity, which may suggest source similarity between sites. The correlation largely depends on season (Figures 9 and S10–S12). The strong correlations for NH_4^+, K^+, SO_4^{2-}, NO_3^-, OC, and EC in the spring and winter infer that basin and plateau sites share similar sources for the species, while weak correlations for NO_3^-, OC, and EC in summer and fall indicate dissimilar sources impacts between Sichuan Basin and Tibetan Plateau.

Compared with the species from anthropogenic sources, the lowest CV values for Na^+, Mg^{2+}, and Ca^{2+} among the species indicated that they are more comparable between basin and plateau sites. Furthermore, changes in Na^+ values are more synchronous than Mg^{2+} and Ca^{2+} in summer and fall. Na^+ concentration is found to be high in salt-rich dust from saline soils (Quick and Chadwick, 2011). Dust events frequently occurred in spring and winter over Tibetan Plateau and Northwest China where saline and alkaline land and dried salt-lakes located (Jiang et al., 2021; Zhang et al., 2009; Zhang et al., 2021), and thus the weak correlations for Na^+, Mg^{2+}, and Ca^{2+} values in spring and winter may suggest local and regional dust plume impacts. Therefore, the lack of considering mineral dust impacts in separation of BrC light absorption from total aerosol absorption (Eq. 5) might cause some errors. The errors should be much smaller as compared to the studies at north or northeast TP close to Taklimakan and Gobi Deserts.

MODIS active fire data suggests that biomass burning is mainly located in South Asia around our study regions, which is more abundant in cold than warm seasons during our campaign (Figure S13). The PM mass concentrations in conjunction with wind data can be used to identify the local PM origins, and Figure 10 shows K^+ pollution rose in the four seasons at the six sites. The back trajectory calculation can give PM origins from long-range transport, and Figures 11 and S14-S16 illustrate the gridded back trajectory frequencies in the four seasons. K^+ stratification in warm seasons is more obvious than that in cold seasons, which infers that there are more biomass burning plumes over Tibetan Plateau in spring and winter. The change in wind direction is not obvious from Sichuan Basin to Tibetan Plateau in warm seasons. However, the predominant wind direction is northwest–southeast in cold seasons for the basin sites, while that mainly focuses on southwest for the plateau sites (Figure 10). The highest frequency of back trajectory also is in southwest of the sampling sites in winter (Figure 11). Therefore, the biomass burning emissions originated from South Asia are transported to eastern Tibetan Plateau by highly frequent southwesterly winds, and thus induce high K^+ concentrations in spring and winter. The BrC aerosols from the intensive biomass burning in South Asia are gradually aged by internal or external mixing with the other anthropogenic emissions during the long-range transport. The light absorption of the aged BrC aerosols over the TP is enhanced by coating the inorganic components (Zhang et al., 2022), which may partly contribute to the stronger BrC light absorption at the plateau sites than the basin sites. Unlike the eastern TP, the carbonaceous aerosols in western SCB are

regionally transported from the central and eastern SCB, which can be seen from pollution rose and back trajectories. The aerosols accumulate and stagnate at the front areas of the mountains due to terrain block, and thus the light absorption of EC aerosols emitted from motor vehicles is enhanced by the intensive mixing among the air pollutants.

4 Summary and conclusions

Tibetan Plateau (TP) is surrounded by the three highly polluted regions, i.e., Indo-Gangetic Plain (IGP), Taklimakan and Gobi Deserts (TGDs) and SiChuan Basin (SCB). However, the previous studies mainly focused on the south (IGP) and north slopes (TGDs), and thus the first *in-situ* aerosol measurements were conducted at eastern slope of Tibetan Plateau (ESTP) to study the elevation-dependent light absorption of carbonaceous aerosols from the highly polluted SCB to the pristine TP. The source and origin impacts on light absorption of aerosols also were discussed by combining with PMF and HYSPLIT results.

The EC and BrC light absorption was separated by the simple two-component model. The BrC light absorption coefficient at 405 nm accounting for that of total carbon (TC, sum of EC and BrC) is found to increase from ~ 20% inside the SCB to ~ 50% over the TP. The BrC mass absorption efficiency (MAE) over eastern TP is 2–3 times higher than that inside the SCB with strong elevation-dependent absorption. The most significant elevation-dependent winter MAE_{BrC} is closely related to the high ratio of secondary to primary organic carbon (OC), i.e., more OC from secondary formation than primary emissions at high altitudes. Different from BrC, winter MAE_{EC} declines from the highly polluted SCB to clean TP, which is due to source difference between the two regions. More urban sources (vehicles, industries, etc.) are trapped inside the deep SCB due to poor dispersion and frequent temperature inversion in cold seasons. The high primary emissions and weak dispersion conditions are favorable for mixing and aerosol aging to enhance light absorption inside the basin. The median radiative forcing of BrC relative to EC increases from about 0.10 inside the basin to 0.42 over eastern TP, which is associated with OC/EC ratio. Therefore, the enhanced radiative forcing of BrC relative to EC is because the concentration of OC decreases more slowly with altitude than does EC.

The first aerosol field experiment was conducted at the specific study region, but only six sampling

sites were used from the deep SCB to eastern TP in this study. The more measurement sites will be established to better understand the chemical composition and light properties of aerosols at the unique region. The light absorption coefficients and efficiencies of BrC failed to be separated from that of TC in summer and fall at Maerkang and Hongyuan due to instrument failure, which limited to reveal the elevation-dependent light absorption. Furthermore, replacing BrC, OC mass concentration was used to estimate MAE_{BrC}, which may cause large uncertainty, and thus these are expected to be corrected in the future study.

Data availability. Raw data sets (Zhao et al., 2022, DOI: 10.5281/zenodo.6474199) used in this manuscript were available at https://zenodo.org/record/6474199#.YmCn_YtByUk.

Author contributions. Suping Zhao and Ye Yu designed the study. Suping Zhao analyzed the data with help from Ye Yu, Jinbei Chen and Shichang Kang. Daiying Yin and Longxiang Dong collected and analyzed data during the campaign. Shaofeng Qi conducted the field experiment.

Competing interests. The authors declare that they have no conflict of interest.

Financial support. This work was supported by the National Natural Science Foundation of China (42075185; 41605103), Youth Innovation Promotion Association, CAS (Y2021111), and Gansu Science and Technology Program key projects (20JR10RA037 and 18JR2RA005).

References

Bond, T. C.: Spectral dependence of visible light absorption by carbonaceous particles emitted from coal combustion, Geophysical Research Letters, 28(21), 4075–4078, 2001.

Bond, T. C., Streets, D. G., Yarber, K. F., Nelson, S. M., Woo, J. H., and Klimont, Z.: A technology-based global inventory of black and organic carbon emissions from combustion, Journal of Geophysical Research: Atmospheres, 109(D14), D14203, 2004.

Chen, Y., Xie, S. D., Luo, B., and Zhai, C. Z.: Characteristics and origins of carbonaceous aerosol in the Sichuan Basin, China, Atmospheric Environment, 94, 215–223, 2014.

Chen, L. W. A., Chow, J. C., Wang, X. L., Robles, J. A., Sumlin, B. J., Lowenthal, D. H., Zimmermann,

R., and Watson, J. G.: Multi-wavelength optical measurement to enhance thermal/optical analysis for carbonaceous aerosol, Atmospheric Measurement Techniques, 8(1), 451–461, 2015.

Chen, P. F., Kang, S. C., Tripathee, L., Ram, K., Rupakheti, M., Panday, A. K., Zhang, Q. G., Guo, J. M., Wang, X. X., Pu, T., and Li, C. L.: Light absorption properties of elemental carbon (EC) and water-soluble brown carbon (WS–BrC) in the Kathmandu Valley, Nepal: A 5-year study, Environmental Pollution, 261, 114239, 2020.

Choudhary, V., Rajput, P., Singh, D. K., Singh, A. K., and Gupta, T.: Light absorption characteristics of brown carbon during foggy and non-foggy episodes over the Indo-Gangetic Plain, Atmospheric Pollution Research, 9(3), 494–501, 2018.

Chow, J. C., Watson, J. G., Chen, L.-W. A., Chang, M. C. O., Robinson, N. F., Trimble, D., and Kohl, S.: The IMPROVE_A Temperature Protocol for Thermal/Optical Carbon Analysis: Maintaining Consistency with a Long-Term Database, Journal of the Air & Waste Management Association, 57(9), 1014–1023, 2007.

Chung, C. E., Ramanathan, V., and Decremer, D.: Observationally constrained estimates of carbonaceous aerosol radiative forcing, Proceedings of the National Academy of the Sciences of the United States of America, 109(29), 11624–11629, 2012.

Cong, Z. Y. , Kang, S. C., Smirnov, A., and Holben, B.: Aerosol optical properties at Nam Co, a remote site in central Tibetan Plateau, Atmospheric Research, 92(1), 42−48, 2009.

Cong, Z. Y., Kang, S. C., Kawamura, K., Liu, B., Wan, X., Wang, Z., Gao, S., and Fu, P.: Carbonaceous aerosols on the south edge of the Tibetan Plateau: concentrations, seasonality and sources, Atmospheric Chemistry and Physics, 15(3), 1573–1584, 2015.

Cui, X. Q., Ren, J. W., Wang, Z. B., Yu, G. M., and Yue, G. Y.: Soluble ions in atmospheric $PM_{2.5}$ over glacier terminus determined by ion chromatography and source analysis, Journal of Glaciology and Geocryology, 41(3), 574–578, 2019 (in Chinese).

Duan, A. M., and Wu, G. X.: Change of cloud amount and the climate warming on the Tibetan Plateau, Geophysical Research Letters, 33(22), L22704, 2006.

Draxler, R., Stunder, B. Rolph, G., Stein, A., and Taylor, A.: Hybrid Single–Particle Lagrangian Integrated Trajectories (HYsplit): Version 4.9–User's Guide and Model Description, 2009.

Feng, X. Y, Wei, S. M, and Wang, S. G.: Temperature inversions in the atmospheric boundary layer and lower troposphere over the Sichuan Basin, China: Climatology and impacts on air pollution, Science of

the Total Environment, 726, 138579, 2020.

Gao, Y. H., Chen, F., Lettenmaier, D. P., Xu, J. W., Xiao, L. H., and Li, X.: Does elevation-dependent warming hold true above 5000 m elevation? Lessons from the Tibetan Plateau, npj Climate and Atmospheric Science, 1, 19, 2018.

Garrett, T. J., and Zhao, C. F.: Increased Arctic cloud longwave emissivity associated with pollution from mid-latitudes, *Nature*, 440(7085), 787–789, 2006.

Guo, D. L., Sun, J. Q., Yang, K., Pepin, N., and Xu, Y. M.: Revisiting recent elevation-dependent warming on the Tibetan Plateau using satellite-based data sets, Journal of Geophysical Research: Atmospheres, 124(15), 8511–8521, 2019.

Guo, D. L., Pepin, N., Yang, K., Sun, J. Q., and Li, D.: Local changes in snow depth dominate the evolving pattern of elevation-dependent warming on the Tibetan Plateau, Science Bulletin, 66(11), 1146–1150, 2021.

Han, T. T., Liu, X. G., Zhang, Y. H., Gu, J. W., Tian, H. Z., Zeng, L. M., Chang, S.-Y., Cheng, Y. F., Lu, K. D., and Hu, M.: Chemical characteristics of PM_{10} during the summer in the mega-city Guangzhou, China, Atmospheric Research, 137, 25–34, 2014.

Huang, J. P., Minnis, P., Yi, Y. H., Tang, Q., Wang, X., Hu, Y. X., Liu, Z. Y., Ayers, K., Trepte, C., and Winker, D.: Summer dust aerosols detected from CALIPSO over the Tibetan Plateau, Geophysical Research Letters, 34(18), L18805, 2007.

Huang, R. J., Yang, L., Cao, J. J., Chen, Y., Chen, Q., Li, Y. J., Duan, J., Zhu, C. S., Dai, W. T., Wang, K., Lin, C. S., Ni, H. Y., Corbin, J. C., Wu, Y. F., Zhang, R. J., Tie, X. X., Hoffmann, T., O'Dowd, C., and Dusek, U.: Brown carbon aerosol in urban Xi'an, Northwest China: the composition and light absorption properties, Environmental Science and Technology, 52(12), 6825–6833, 2018.

Jiang, Y. S., Gao, Y. H., He, C. L., Liu, B. L., Pan, Y. J., and Li, X.: Spatiotemporal distribution and variation of wind erosion over the Tibetan Plateau based on a coupled land-surface wind-erosion model, Aeolian Research, 50, 100699, 2021.

Kang, S. C., Zhang, Q. G., Qian, Y., Ji, Z. M., Li, C. L., Cong, Z. Y., Zhang, Y. L., Guo, J. M., Du, W. T., Huang, J., You, Q. L., Panday, A. K., Rupakheti, M., Chen, D. L., Gustafsson, O., Thiemens, M. H., and Qin, D. H.: Linking atmospheric pollution to cryospheric change in the Third Pole region: current progress and future prospects, National Science Review, 6(4), 796–809, 2019.

Kang, S. C., Zhang, Y. L., Qian, Y., and Wang, H. L.: A review of black carbon in snow and ice and its

impact on the cryosphere, Earth-Science Reviews, 210, 103346, 2020.

Kawamura, K., Kasukabe, H., and Barrie, L. A.: Secondary formation of water-soluble organic acids and alpha-dicarbonyls and their contributions to total carbon and water-soluble organic carbon: Photochemical aging of organic aerosols in the Arctic spring, Journal of Geophysical Research: Atmospheres, 115, D21306, 2010.

Lau, W. K. M., Kim, M. K., Kim, K. M., and Lee, W. S.: Enhanced surface warming and accelerated snow melt in the Himalayas and Tibetan Plateau induced by absorbing aerosols, Environmental Research Letters, 5, 025204, 2010.

Li, C. L., Chen, P. F., Kang, S C., Yan, F. P., Hu, Z., Qu, B., and Sillanpää, M.: Concentrations and light absorption characteristics of carbonaceous aerosol in $PM_{2.5}$ and PM_{10} of Lhasa city, the Tibetan Plateau, Atmospheric Environment, 127, 340–346, 2016.

Liu, X. D., and Chen, B. D.: Climatic warming in the Tibetan Plateau during recent decades, International Journal of Climatology, 20(14), 1729–1742, 2000.

Liu, H., Pan, X. L., Liu, D. T., Liu, X., Chen, X., Tian, Y., Sun, Y. L., Fu, P. Q., and Wang, Z. F.: Mixing characteristics of refractory black carbon aerosols at an urban site in Beijing, Atmospheric Chemistry and Physics, 20, 5771–5785, 2020.

Liu, J. M., Scheuer, E., Dibb, J., Ziemba, L. D., Thornhill, K. L., Anderson, B. E., Wisthaler, A., Mikoviny, T., Devi, J. J., Bergin, M., and Weber, R. J.: Brown carbon in the continental troposphere, Geophysical Research Letters, 41, 2191–2195, 2014.

Liu, J., Scheuer, E., Dibb, J., Diskin, G. S., Ziemba, L. D., Thornhill, K. L., Anderson, B. E., Wisthaler, A., Mikoviny, T., Devi, J. J., Bergin, M., Perring, A. E., Markovic, M. Z., Schwarz, J. P., Campuzano-Jost, P., Day, D. A., Jimenez, J. L., and Weber, R. J.: Brown carbon aerosol in the North American continental troposphere: Sources, abundance, and radiative forcing, Atmospheric Chemistry and Physics, 15, 7841–7858, 2015.

Levinson, R., Akbari, H., and Berdahl, P.: Measuring solar reflectance—part I: defining a metric that accurately predicts solar heat gain, Solar Energy, 84(9), 1717–1744, 2010.

Lu, A. G., Kang, S. C., Li, Z. X., and Theakstone, W. H.: Altitude effects of climatic variation on Tibetan Plateau and its vicinities, Journal of Earth Science, 21(2), 189–198, 2010.

Mountain Research Initiative EDW Working Group.: Elevation-dependent warming in mountain regions of the world, Nature Climate Change, 5(5), 424–430, 2015.

Olson, M. R., Garcia, M. V., Robinson, M. A., Rooy, P. V., Dietenberger, M. A., Bergin, M., and Schauer, J. J.: Investigation of black and brown carbon multiple-wavelength dependent light absorption from biomass and fossil fuel combustion source emissions, Journal of Geophysical Research: Atmospheres, 120(13), 6682–6697, 2015.

Palazzi, E., Filippi, L., and von Hardenberg, J.: Insights into elevation-dependent warming in the Tibetan Plateau-Himalayas from CMIP5 model simulations, Climate Dynamics, 48 (11), 3991–4008, 2017.

Peng, C., Yang, F. M., Tian, M., Shi, G. M., Li, L., Huang, R. J., Yao, X. J., Luo, B., Zhai, C. Z., and Chen, Y.: Brown carbon aerosol in two megacities in the Sichuan Basin of southwestern China: Light absorption properties and implications, Science of the Total Environment, 719, 137483, 2020a.

Peng, C., Tian, M., Wang, X. L., Yang, F. M., Shi, G. M., Huang, R. J., Yao, X. J., Wang, Q. Y., Zhai, C. Z. Zhang, S. M., Qian, R. Z., Cao, J. J., and Chen, Y.: Light absorption of brown carbon in $PM_{2.5}$ in the Three Gorges Reservoir region, southwestern China: Implications of biomass burning and secondary formation, Atmospheric Environment, 229, 117409, 2020b.

Pepin, N., Deng, H. J., Zhang, H. B., Zhang, F., Kang, S. C., and Yao, T. D.: An examination of temperature trends at high elevations across the Tibetan Plateau: The use of MODIS LST to understand patterns of elevation-dependent warming, Journal of Geophysical Research: Atmospheres, 124(11), 5738–5756, 2019.

Quick, D. J., and Chadwick, O. A.: Accumulation of salt-rich dust from Owens Lake playa in nearby alluvial soils, Aeolian Research, 3(1), 23–29, 2011.

Ramanathan, V., and Carmichael, G.: Global and regional climate changes due to black carbon, Nature Geoscience, 1(4), 221–227, 2008.

Rangwala, I., and Miller, J. R.: Climate change in mountains: a review of elevation-dependent warming and its possible causes, Climatic Change, 114(3-4), 527–547, 2012.

Srinivas, B., Rastogi, N., Sarin, M. M., Singh, A., and Singh, D.: Mass absorption efficiency of light absorbing organic aerosols from source region of paddy-residue burning emissions in the Indo-Gangetic Plain, Atmospheric Environment, 125, 360–370, 2016.

Tao, J., Zhang, L. M., Zhang, R. J., Wu, Y. F., Zhang, Z. S., Zhang, X. L., Tang, Y. X., Cao, J. J., and Zhang, Y. H.: Uncertainty assessment of source attribution of $PM_{2.5}$ and its water-soluble organic carbon content using different biomass burning tracers in positive matrix factorization analysis-a case

study in Beijing, China, Science of the Total Environment, 543, 326–335, 2016.

Tian, P. F., Zhang, L., Ma, J. M., Tang, K., Xu, L. L., Wang, Y., Cao, X. J., Liang, J. N., Ji, Y. M., Jiang, J. H., Yung, Y. L., and Zhang, R. Y.: Radiative absorption enhancement of dust mixed with anthropogenic pollution over East Asia, Atmospheric Chemistry and Physics, 18(11), 7815–7825, 2018.

Turpin, B. J., and Lim, H. J.: Species contributions to $PM_{2.5}$ mass concentrations: revisiting common assumptions for estimating organic mass, Aerosol Science and Technology, 35(1), 602−610, 2001.

Viidanoja, J., Sillanpaa, M., Laakia, J., Kerminen, V. M., Hillamo, R., Aarnio, P., and Koskentalo, T.: Organic and black carbon in $PM_{2.5}$ and PM_{10}: 1 year of data from an urban site in Helsinki, Finland, Atmospheric Environment, 36(19), 3183−3193, 2002.

Wang, H. B., Tian, M., Chen, Y., Shi, G. M., Liu, Y., Yang, F. M., Zhang, L. M., Deng, L. Q., Yu, J., Peng, C., and Cao, X. Y.: Seasonal characteristics, formation mechanisms and source origins of $PM_{2.5}$ in two megacities in Sichuan Basin, China, Atmospheric Chemistry and Physics, 18(2), 865−881, 2018.

Wang, Y. J., Hu, M., Hu, W., Zheng, J., Niu, H. Y., Fang, X., Xu, N., Wu, Z. J., Guo, S., Wu, Y. S., Chen, W. T., Lu, S. H., Shao, M., Xie, S. D., Luo, B., and Zhang, Y. H.: Secondary formation of aerosols under typical high-humidity conditions in wintertime Sichuan Basin, China: A contrast to the North China Plain, Journal of Geophysical Research: Atmospheres, 126(10), e2021JD034560, 2021.

Wilson, J. G., Kingham, S., Pearce, J., and Sturman, A. P.: A review of intraurban variations in particulate air pollution: implications for epidemiological research, Atmospheric Environment, 39(34), 6444−6462, 2005.

Wu, G. M., Wan, X., Gao, S. P., Fu, P. Q., Yin, Y. G., Li, G., Zhang, G. S., Kang, S. C., Ram, K., and Cong, Z. Y.: Humic-like substances (HULIS) in aerosols of central Tibetan Plateau (Nam Co, 4730 m asl): abundance, light absorption properties, and sources, Environmental Science and Technology, 52(13), 7203−7211, 2018.

Xu, B. Q., Cao, J. J., Hansen, J., Yao, T. D., Joswia, D. R., Wang, N. L., Wu, G. J., Wang, M., Zhao, H. B., Yang, W., Liu, X. Q., and He, J. Q.: Black soot and the survival of Tibetan glaciers, Proceedings of the National Academy of the Sciences of the United States of America, 106(52), 22114–22118, 2009.

Yin, D. Y., Zhao, S. P., Qu, J. J., Yu, Y., Kang, S. C., Ren, X. L., Zhang, J., Zou, Y., Dong, L. X., Li, J. L., He, J. J., Li, P., and Qin, D. H.: The vertical profiles of carbonaceous aerosols and key influencing factors during wintertime over western Sichuan Basin, China, Atmospheric Environment, 223, 117269, 2020.

You, Q. L., Chen, D. L., Wu, F. Y., Pepin, N., Cai, Z. Y., Ahrens, B., Jiang, Z. H., Wu, Z. W., Kang, S. C., and AghaKouchak A.: Elevation dependent warming over the Tibetan Plateau: Patterns, mechanisms and perspectives, Earth-Science Reviews, 210, 103349, 2020.

Zeng, L. H., Zhang, A. X., Wang, Y. H., Wagner, N. L., Katich, J. M., Schwarz, J. P., Schill, G. P., Brock, C., Froyd, K. D., Murphy, D. M., Williamson, C. J., Kupc, A., Scheuer, E., Dibb, J., and Weber, R. J.: Global measurements of brown carbon and estimated direct radiative effects, Geophysical Research Letters, 47(13), e2020GL088747, 2020.

Zhang, J., Wang, Y. Y., Teng, X. M., Liu, L., Xu, Y. S., Ren, L. H., Shi, Z. B., Zhang, Y., Jiang, J. K., Liu, D. T., Hu, M., Shao, L. Y., Chen, J. M., Martin, S. T., Zhang, X. Y., and Li, W. J.: Liquid-liquid phase separation reduces radiative absorption by aged black carbon aerosols, Communications Earth & Environment, 3, 128, 2022.

Zhang, L., Tang, C. G., Huang, J. P., Du, T., Guan, X., Tian, P. F., Shi, J. S., Cao, X. J., Huang, Z. W., Guo, Q., Zhang, H. T., Wang, M., Zeng, H. Y., Wang, F. Y., and Dolkar, P.: Unexpected high absorption of atmospheric aerosols over a western Tibetan Plateau site in summer, Journal of Geophysical Research: Atmospheres, 126(7), e2020JD033286, 2021.

Zhang, X. Y., Zhuang, G. S., Yuan, H., Rahn, K. A., Wang, Z. F., and An, Z. S.: Aerosol particles from dried salt-lakes and saline soils carried on dust storms over Beijing, Terrestrial Atmospheric and Oceanic Sciences, 20(4), 619–628, 2009.

Zhang, Y. Z., Forrister, H., Liu, J. M., Dibb, J., Anderson, B., Schwarz, J. P., Perring, A. E., Jimenez, J. L., Campuzano-Jost, P., Wang, Y. H., Nenes, A., and Weber, R. J.: Top-of-atmosphere radiative forcing affected by brown carbon in the upper troposphere, Nature Geoscience, 10(7), 486–489, 2017.

Zhao, C. F., Yang, Y. K., Fan, H., Huang, J. P., Fu, Y. F., Zhang, X. Y., Kang, S. C., Cong, Z. Y., Letu, H., and Menenti, M.: Aerosol characteristics and impacts on weather and climate over the Tibetan Plateau, National Science Review, 7(3), 492–495, 2020.

Zhao, S. P., Yu, Y., Yin, D. Y., Qin, D. H., He, J. J., and Dong, L. X.: Spatial patterns and temporal variations of six criteria air pollutants during 2015 to 2017 in the city clusters of Sichuan Basin, China, Science of the Total Environment, 624, 540–557, 2018.

Zhao, S. P., Yin, D. Y., Yu, Y., Kang, S. C., Ren, X. L., Zhang, J., Zou, Y., and Qin, D. H.: PM_1 chemical composition and light absorption properties in urban and rural areas within Sichuan Basin, southwest China, Environmental Pollution, 280, 116970, 2021.

Zhao, S. P., Qi, S. F., Yu, Y., Kang, S. C., Dong, L. X., Chen, J. B., and Yin, D. Y.: Measurement report: The first *in-situ* PM1 chemical measurements at the steep slope from highly polluted Sichuan Basin to pristine Tibetan Plateau: light absorption of carbonaceous aerosols, and source and origin impacts [data set], https://doi.org/10.5281/zenodo.6474199, 2022.

Zhao, S. Y., Feng, T., Tie, X. X., and Wang, Z. B.: The warming Tibetan Plateau improves winter air quality in the Sichuan Basin, China, Atmospheric Chemistry and Physics, 20(23), 14873–14887, 2020.

Zhao, Z. Z., Cao, J. J, Chow, J. C., Watson, J. G., Chen, A. L.-W., Wang, X. L., Wang, Q. Y., Tian, J., Shen, Z. X., Zhu, C. S., Liu, S. X., Tao, J., Ye, Z. L., Zhang, T., Zhou, J. M., and Tian, R. X.: Multi-wavelength light absorption of black and brown carbon at a high-altitude site on the Southeastern margin of the Tibetan Plateau, China, Atmospheric Environment, 212, 54–64, 2019.

Zhu, C. S., Cao, J. J., Huang, R. J., Shen, Z. X., Wang, Q. Y., and Zhang, N. N.: Light absorption properties of brown carbon over the southeastern Tibetan Plateau, Science of the Total Environment, 625, 246–251, 2018.

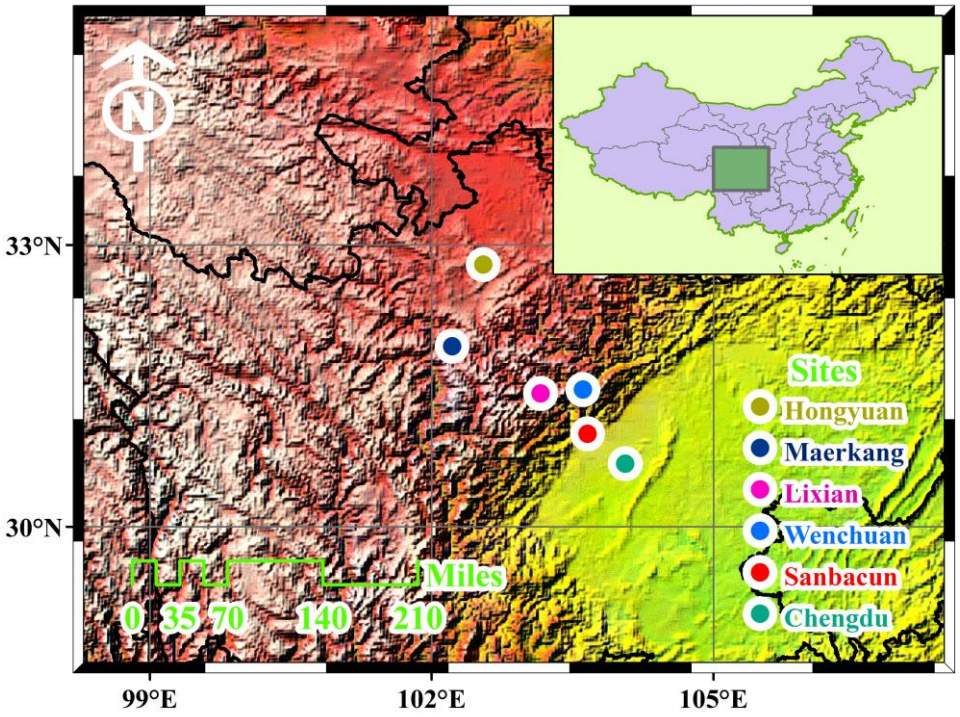

Figure 1: Geographic location of the six *in-situ* measurement sites (Chengdu, Sanbacun, Wenchuan, Lixian, Maerkang, and Hongyuan) along the eastern slope of Tibetan Plateau. The map is a pure reproduction of Google Maps with added a marks for our study locations.

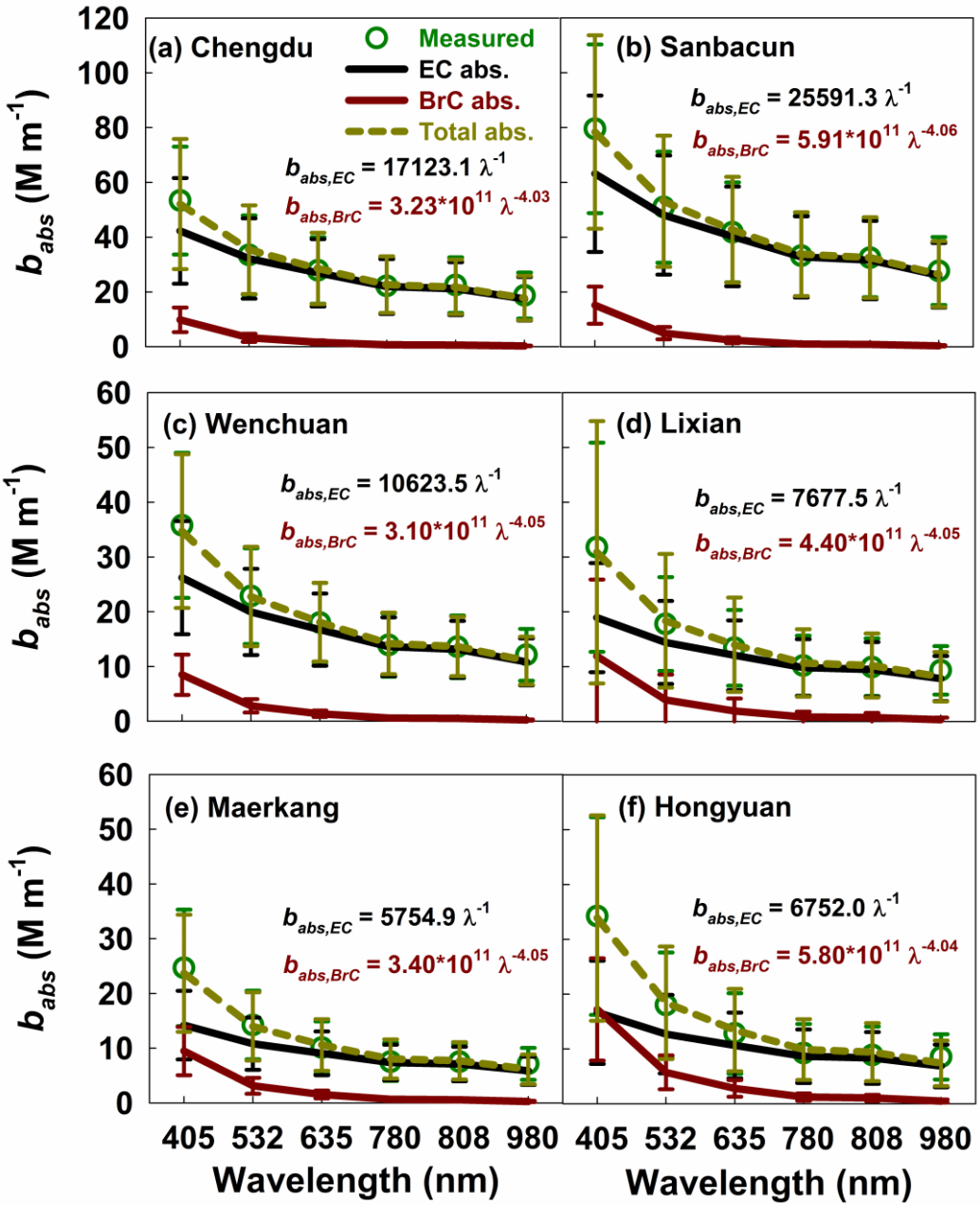

Figure 2: Spectral light absorption coefficients (b_{abs}) by EC and BrC in spring and winter at the six sites along the ESTP. The subplots depict the decomposition of total light absorption by EC and BrC with the model given in Eq. 4. Error bars represent uncertainties derived from replicate analyses and lower quantifiable limits.

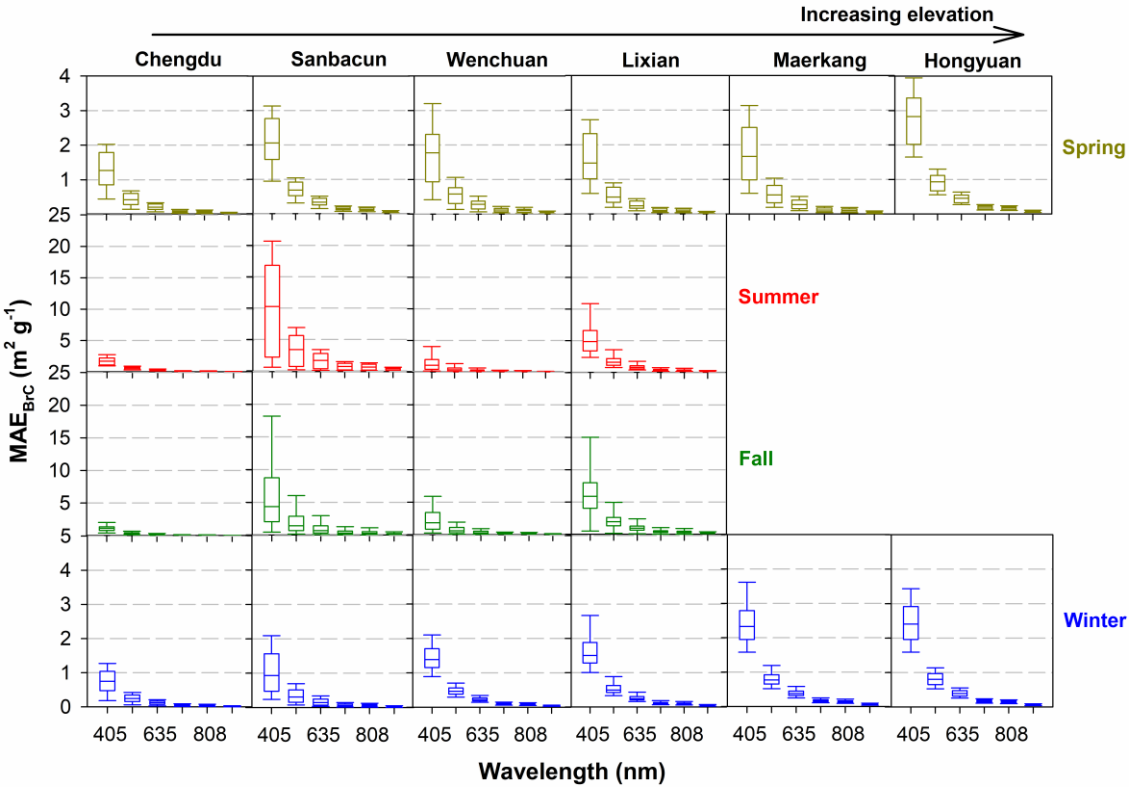

Figure 3: Box plots of spectral BrC mass absorption efficiency (MAE_{BrC}) in each season from Chengdu inside the SCB to Hongyuan over the TP extending elevation from 500 m to 3500 m. The lines inside the boxes denote the median values, and the two whiskers and the top and bottom of the boxes denote the 5th and 95th and the 75th and 25th percentiles.

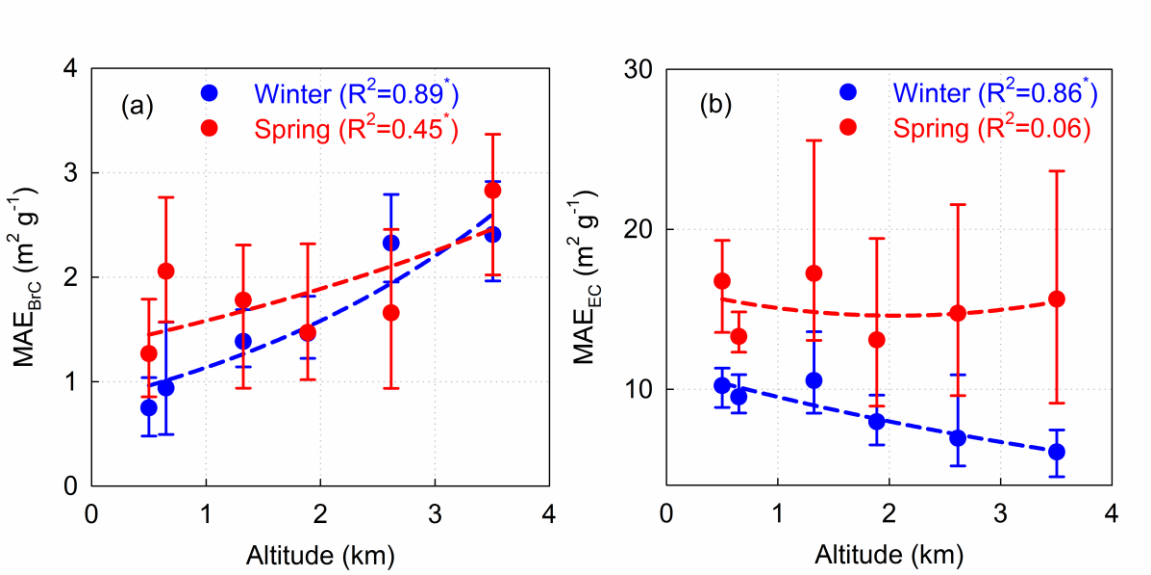

Figure 4: Variations of (a) MAE_{BrC} and (b) MAE_{EC} at 405 nm as altitude in spring and winter during the campaign. The solid dots denote the median values, and the two whiskers of the dots denote the 25th and 75th percentiles. The relationships between averaged MAE and altitude of the measurement sites were fitted by exponential function, and the coefficients of determination (R^2) also were given in each subplot. The relationships (R^2 with the superscript of an asterisk) passed the significance level of 0.01.

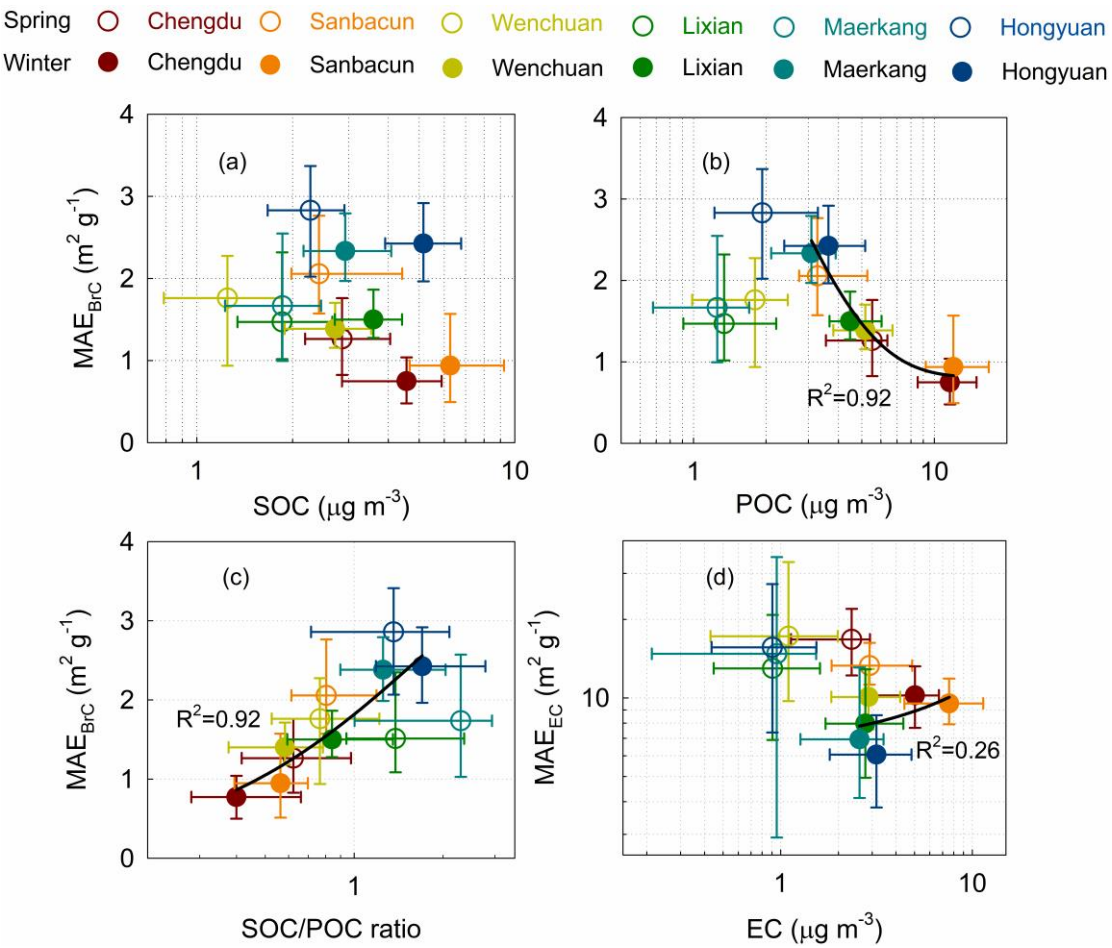

Figure 5: Variations of spring and winter mean MAE_{BrC} as (a) SOC, (b) POC, (c) SOC/POC ratio and (d) MAE_{EC} as EC concentrations at the six sites. The hollow and solid dots denote the median values in spring and winter, and the four whiskers of the dots denote the 25th and 75th percentiles of the corresponding two variables. The horizontal axis in each subplot is showed on a logarithmic scale to more clearly see the details.

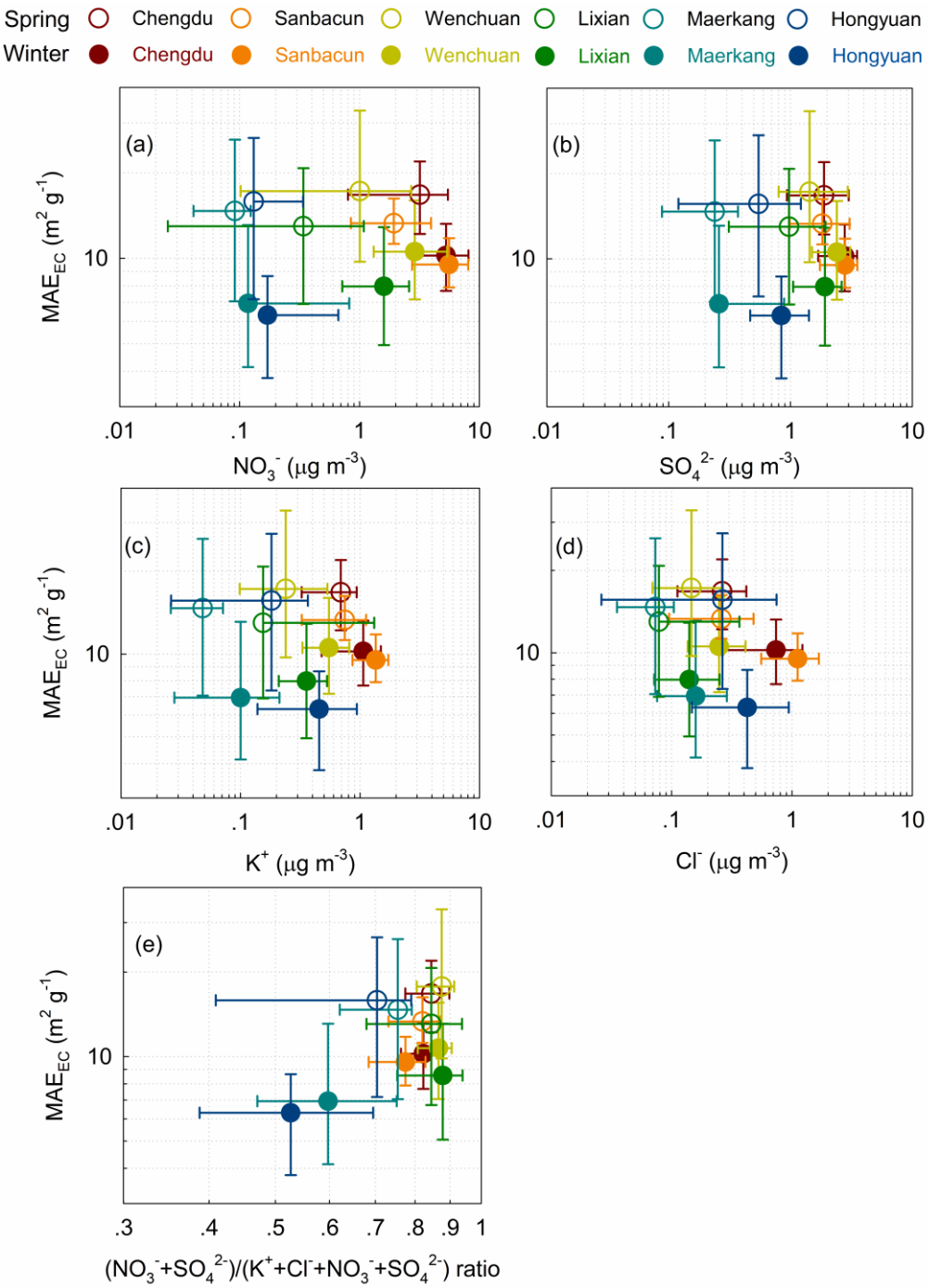

Figure 6: Variations of spring and winter MAE_{EC} as (a) NO_3^-, (b) SO_4^{2-}, (c) K^+, and (d) Cl^- concentrations, and (e) $(NO_3^-+ SO_4^{2-})$ / $(K^+ + Cl^- + NO_3^- + SO_4^{2-})$ ratio at the six sites. The hollow and solid dots denote the median values in spring and winter, and the four whiskers of the dots denote the 25th and 75th percentiles of the corresponding two variables. The axes in each subplot are showed on a logarithmic scale to more clearly see the details.

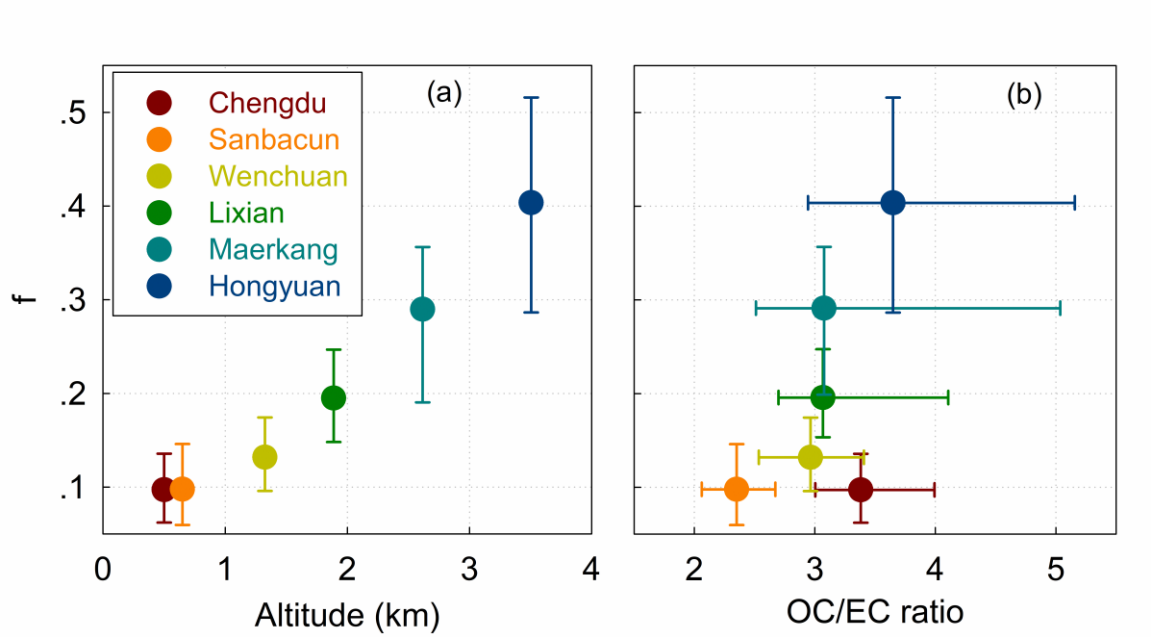

Figure 7: Variation of radiative forcing of BrC relative to EC (f, see Eq. 8) as (a) altitude and (b) OC/EC ratio for each site. The solid dots denote the median values, and the two whiskers of the dots denote the 25th and 75th percentiles of the variables.

5

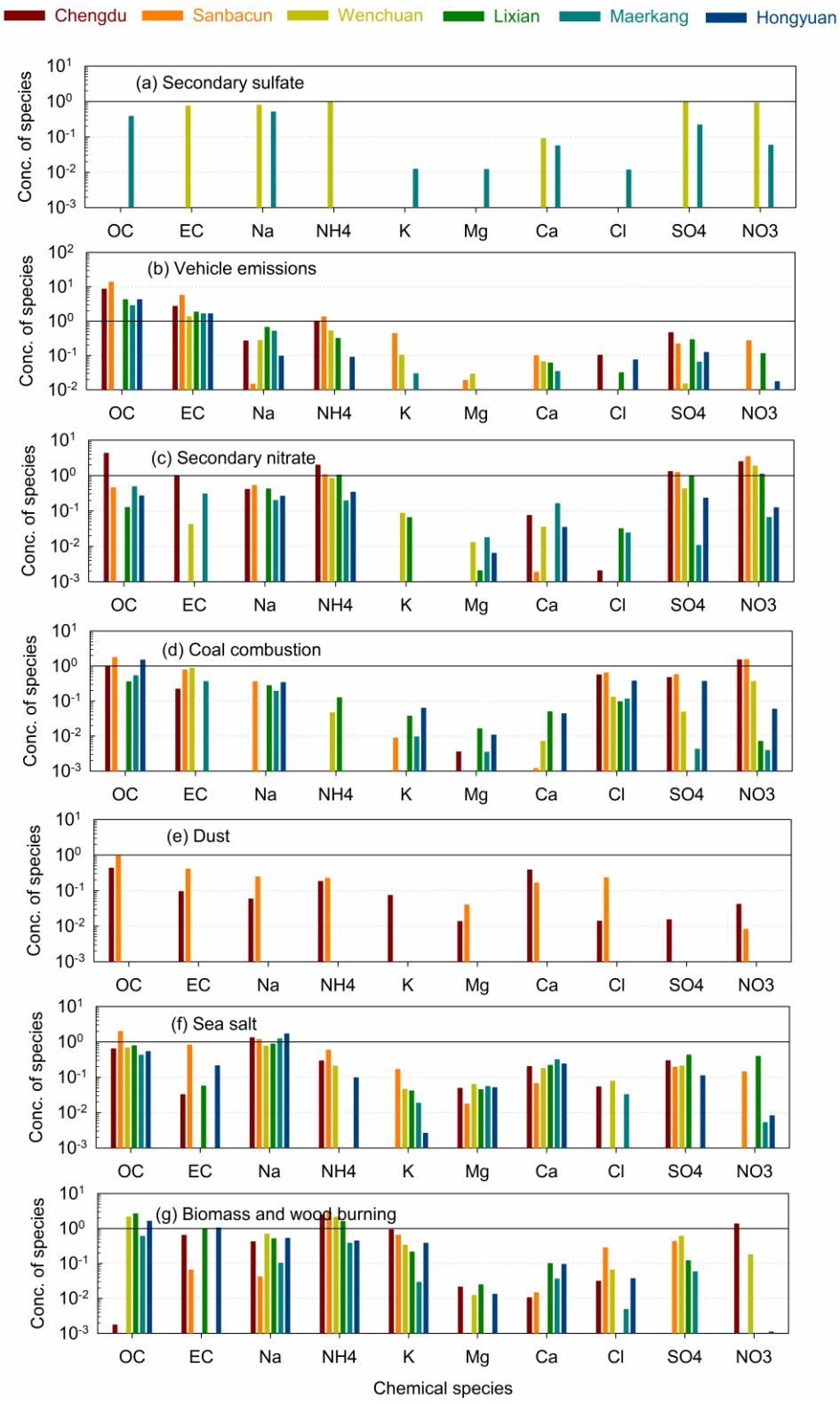

Figure 8: Mass concentrations of species for each source at each site apportioned by PMF model in winter during the campaign. The vertical axes are showed on logarithmic scale to better distinguish the concentrations of chemical species among the measurement sites.

5

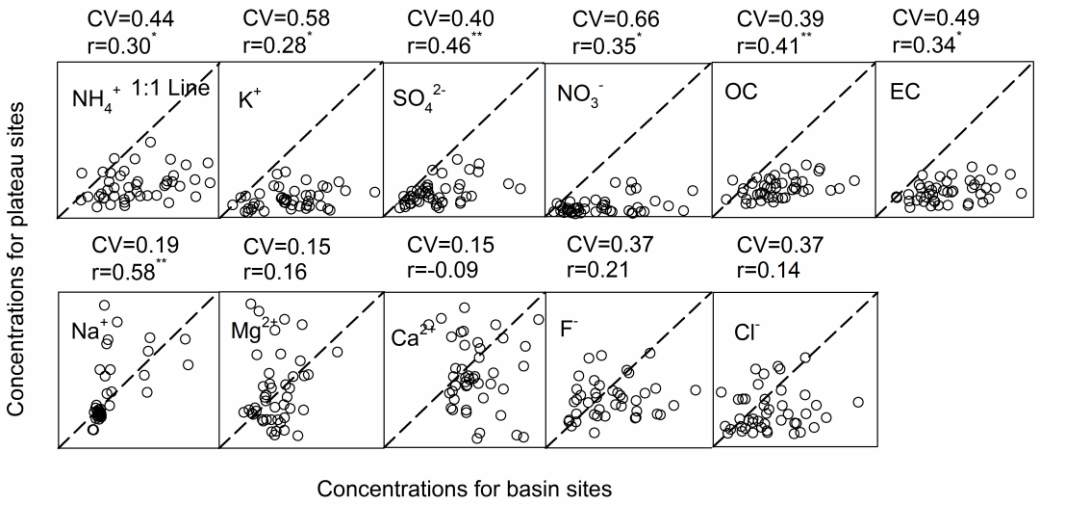

Figure 9: Relationships of spring PM_1 chemical components concentrations between basin (horizontal axes, including Chengdu and Sanbacun) and plateau sites (vertical axes, including Wenchuan, Lixian, Maerkang and Hongyuan). The correlation coefficients (r) with an asterisk and two asterisk superscripts passed the significance level of 0.05 and 0.01, respectively.

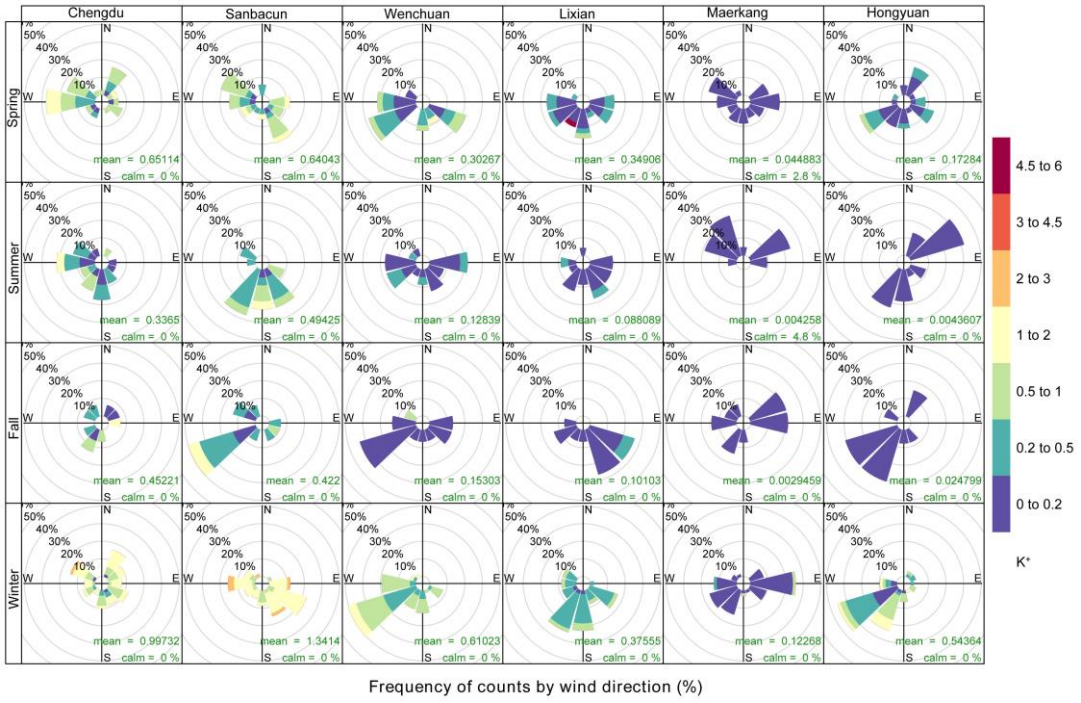

Figure 10: K^+ pollution rose in the four seasons at the six sites along the ESTP. Mean K^+ concentrations and calm frequencies also were given in each subplot.

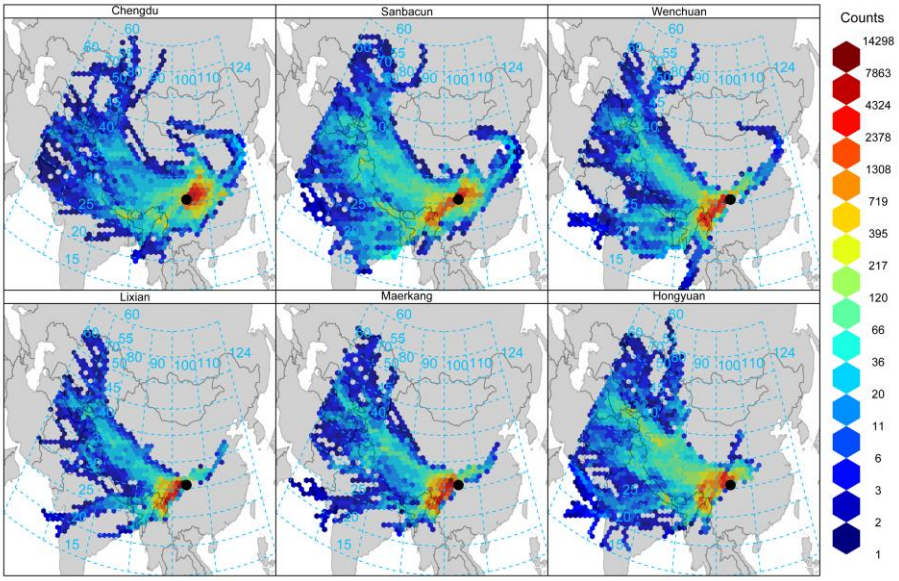

Figure 11: Gridded back trajectory frequencies with hexagonal binning in winter at the six sites from west Sichuan Basin to Tibetan Plateau. The map is a pure reproduction of Google Maps with added the trajectory frequencies. Copyright © Google Maps.

Table 1 Summary of the measurement sites (name, location and altitude).

Name	Latitude (degree)	Longitude (degree)	Altitude (km)
Chengdu	30.67	104.06	0.50
Sanbacun	30.99	103.66	0.65
Wenchuan	31.46	103.61	1.33
Lixian	31.42	103.16	1.89
Maerkang	31.92	102.22	2.62
Hongyuan	32.79	102.55	3.50

Table2 Seasonally average values (mean ± std.) of OC and EC concentrations, light absorption coefficient (b_{abs}), mass absorption efficiency (MAE) and meteorological variables (wind speed (WS), temperature (Tem.), relative humidity (RH)) at the six sites during the measurement campaign. There is no b_{abs} or MAE reported for MEK and HY in summer and fall as the used DRI instrument does not work at the 2 wavelengths of 405 nm and 445 nm when the samples are measured, and thus separation of EC and BrC cannot be conducted by Eq. (5). Chengdu, Sanbacun, Wenchuan, Lixian, Maerkang and Hongyuan are abbreviated as CD, SBC, WC, LX, MEK and HY, respectively.

Season	Sites	OC	EC	b_{abs} (M m^{-1})		MAE (m^2 g^{-1})		WS	Tem.	RH
		(μg m^{-3})	(μg m^{-3})	BrC, 405	EC, 405	BrC, 405	EC, 405	(m s^{-1})	(℃)	(%)
Spring	CD	7.9±3.7	2.2±1.2	8.5±2.8	32.4±12.7	1.3±0.6	17.1±4.8	1.6±0.7	17.5±4.3	80.3±19.9
	SBC	6.7±3.0	3.3±1.5	13.7±5.6	44.2±16.9	2.1±0.9	13.7±2.5	1.4±0.6	16.9±4.1	77.6±15.9
	WC	3.2±1.6	1.2±0.8	4.8±2.3	20.2±9.0	1.6±0.9	21.5±11.6	2.4±1.0	15.1±4.4	65.1±17.4
	LX	3.5±1.4	1.0±0.6	5.4±2.5	11.8±5.5	1.7±0.8	13.8±6.9	1.6±0.5	13.3±5.3	61.5±20.4
	MEK	3.0±1.7	0.8±0.6	4.8±2.7	10.2±3.6	1.9±1.2	16.6±9.4	1.1±0.6	10.6±5.5	62.0±26.5
	HY	4.1±1.6	0.9±0.6	11.5±4.9	12.9±6.2	2.8±0.9	17.3±9.8	2.4±1.0	2.4±3.6	70.0±16.6
Summer	CD	5.4±1.2	1.9±0.5	9.0±2.7	29.2±6.9	1.8±0.6	16.4±4.5	1.3±0.4	25.2±2.9	84.6±18.8
	SBC	2.9±1.2	1.5±0.7	21.8±15.0	32.6±7.9	10.1±7.1	29.8±6.5	1.1±0.4	24.1±3.0	82.7±13.9
	WC	2.2±0.8	1.0±0.5	2.2±1.5	18.9±5.5	1.4±1.3	23.5±9.5	1.7±0.7	23.1±3.2	64.5±16.5
	LX	2.7±0.9	0.8±0.5	13.3±5.0	9.5±2.7	5.4±2.5	16.4±11.3	1.4±0.5	20.9±4.0	65.2±18.0
	MEK	2.7±1.5	0.7±0.6	—	—	—	—	1.0±0.4	16.6±4.3	73.3±22.6
	HY	3.0±1.2	0.8±0.6	—	—	—	—	1.8±0.6	10.1±3.3	77.8±11.6
Fall	CD	4.7±1.3	2.3±1.0	5.3±2.5	40.6±16.6	1.1±0.5	18.3±4.0	1.1±0.4	15.6±4.9	88.4±10.8
	SBC	5.3±3.4	3.0±1.8	22.0±13.7	50.8±11.2	6.0±5.6	24.3±9.3	0.9±0.2	14.9±4.4	89.9±11.6
	WC	1.6±0.8	0.8±0.5	3.0±2.0	18.2±7.3	2.3±1.8	27.3±13.9	1.7±0.6	14.1±5.4	72.7±10.0
	LX	2.4±1.0	0.9±0.5	12.7±6.6	10.5±3.4	6.5±3.8	14.7±10.1	1.3±0.3	11.9±5.6	76.8±11.3
	MEK	2.3±1.2	0.9±0.6	—	—	—	—	0.9±0.4	8.8±5.5	78.4±17.0
	HY	3.4±2.2	1.3±1.1	—	—	—	—	1.9±0.7	0.7±5.6	73.9±11.0
Winter	CD	15.0±5.9	4.7±2.0	10.5±4.6	47.6±20.1	0.8±0.5	10.4±2.8	1.2±0.4	6.6±2.7	78.9±16.9
	SBC	18.9±7.6	7.9±3.4	17.1±10.2	74.7±27.9	1.2±1.0	9.9±2.0	1.0±0.3	5.8±2.7	79.2±15.0
	WC	8.2±3.1	2.8±1.3	11.2±3.2	29.7±9.5	1.5±0.5	11.6±4.4	1.9±0.6	3.6±2.4	60.2±9.0
	LX	8.4±2.7	3.0±1.3	17.1±15.4	24.3±9.1	2.2±2.6	8.9±3.9	1.4±0.4	-0.1±2.1	62.4±10.3
	MEK	5.3±2.3	2.2±1.1	13.2±4.0	16.6±6.3	2.5±0.9	8.6±4.4	1.1±0.3	-0.2±3.7	36.1±11.0
	HY	8.4±3.8	3.0±1.6	21.5±11.3	18.9±10.2	2.5±0.7	6.7±4.9	2.1±1.5	-6.5±6.8	42.8±21.8